Geothermics 63 (2016) 195–209

Contents lists available at ScienceDirect

Geothermics

journal homepage: www.elsevier.com/locate/geothermics

The Basin and Range Dixie Valley Geothermal Wellfield, Nevada, USA—A test bed for developing an Enhanced Geothermal System exploration favorability methodology

Joe Iovenitti[a,*], Fletcher Hank Ibser[b], Matthew Clyne[c], Jon Sainsbury[d], Owen Callahan[e]

[a] Consulting Geoscientist formerly AltaRock Energy, Inc., United States
[b] University of California, Berkeley, United States
[c] Tobii Technology formerly AltaRock Energy Inc., United States
[d] AltaRock Energy Inc., United States
[e] University of Texas, Austin, United States

ARTICLE INFO

Article history:
Received 28 December 2014
Received in revised form
31 December 2015
Accepted 4 January 2016
Available online 11 February 2016

Keywords:
EGS
Exploration
Favorability and trust mapping
Hydrothermal system
Exploration geostatistics

ABSTRACT

The Dixie Valley Geothermal Wellfield (DVGW), a Basin and Range type system in central Nevada USA, is used as an exploration case history for Enhanced Geothermal Systems (EGS). It encompasses an area of approximately 170 km^2. The wellfield produces 67 MW of geothermal power and it contains a number of high temperature non-productive wells. This wellfield was chosen as the calibration site for the development of an EGS exploration methodology due to its extensive body of geoscience data and information on the geothermal system and most importantly, well results in the public domain. This existing body of data (ca. 2011) was in part re-interpreted to produce a baseline conceptual model in terms of a number of serial cross-sections for the available data sets: geology, seismic reflection, resistivity, temperature, gravity-magnetic, and p-wave velocity (*Vp*). The exploration methodology was calibrated against available geothermal well results. Based on a comprehensive review of all available geoscience and well data, EGS favorability maps were generated, from +1 km above sea level (asl) to −4 km asl at 0.5 km intervals, for the three key EGS parameters of interest: rock type, temperature, and stress. Complimentary trust ("confidence-in-the-data-used") maps were also created at the same scale to, among other things, indicate where additional data may be required.

Quantitative geostatistical analysis of the geoscience data was conducted, among other factors, to address the question of whether the baseline geoscience data could be used to predict EGS favorability without the advantage of existing well temperature data. Classification and Regression Tree (CART) was one of a number of geostatistical methods applied to the baseline geoscience data and it provided the most promising results. In CART, the response variable (RV) is predicted while using explanatory variables (EVs). The geoscience parameters (EVs) considered in the CART analysis included temperature, *Vp*, resistivity from magnetotellurics, Coulomb Stress Change (CSC), dilatational strain (from CSC modeling), vertical stress, lithology based on geologic analysis, lithology based on gravity–magnetic modeling (G–M lithology) and the presence or absence of a fault. Temperature increases with depth in the DVGW. Vertical stress also increases with depth and it was deemed as a redundant EV. As such, a CART sensitivity analysis was applied to the baseline data set with and without vertical stress being considered as an EV to determine the effect of removing vertical stress and to evaluate with subsets of EVs that could be predictive of key EGS parameters. R^2-values ranging from 0.611 to 0.841 were obtained for the RVs: temperature, lithology, productive vs. non-productive hydrothermal cells and expected EGS favorable cells (the response variables) using both cross-section and well data and not considering vertical stress. However, these CART results were not used in the generation of the favorability maps because this is the first analysis of its kind that the authors are aware of and more testing at other sites needs to be done; the raw total baseline data set described above was considered the most appropriate for this study.

1. Introduction

Exploration for an Enhanced Geothermal System (EGS) is not unlike exploration for a hydrothermal system with the principal

* Corresponding author.
E-mail addresses: joeiovenitti@comcast.net, joeiovenitti@gmail.com (J. Iovenitti), hank@stat.berkeley.edu (F.H. Ibser), mpclyne@gmail.com (M. Clyne), jonsainsbury@gmail.com (J. Sainsbury), owen.callahan@gmail.com (O. Callahan).

http://dx.doi.org/10.1016/j.geothermics.2016.01.001
0375-6505/

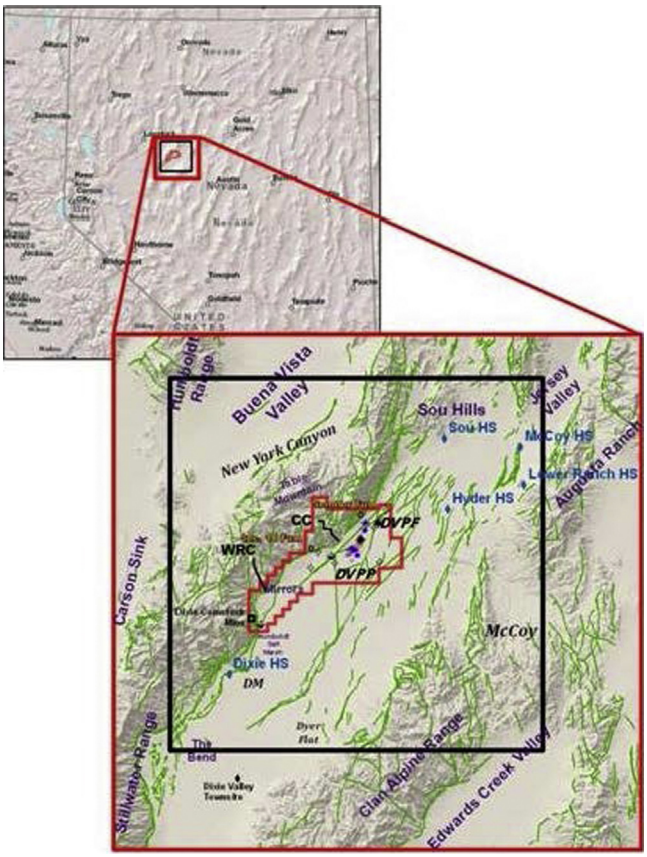

Fig. 1. The Dixie Valley Geothermal Wellfield (DVGW, red irregular outline) in central Nevada, USA encompasses 170 km^2. It lies within a greater project area of 2500 km^2 (black outline). Known and inferred faults are shown in green. Hot springs in the project area are identified along with two major properties within the DVGW: the DVPF: Dixie Valley Producing Field and DVPP: Dixie Valley Power partners. Two fumarolic areas exist in the northwestern portion of the DVGW along the Dixie Valley range-front fault. Within the DVGW, paleo-hot spring sinter deposits and extant fumaroles and hot springs occur locally both along the range-front fault and in its footwall block. The base figure is from Blackwell et al. (2005). (For interpretation of the references to color in this figure legend, the reader is referred to the web version of this article.)

difference being the identification of permeability at depth is not critical for EGS. Three important geoscience parameters for EGS exploration are (1) temperatures greater than 200–250 °C at depths of 1–5 km, (2) brittle rock capable of sustaining fractures at the depth of interest and (3) favorable stress regime at the depth of interest.

This paper draws exclusively from work co-funded by the U.S. Department of Energy Geothermal Technologies Program and AltaRock Energy Inc., under the American Recovery and Reinvestment Act (ARRA) United States Department of Energy contract no. DE-EE0002778. The project involved developing a calibrated EGS exploration methodology using the Dixie Valley Geothermal Wellfield (DVGW), a Basin and Range (B&R) type high temperature geothermal field in central Nevada, United States of America (USA), as a field laboratory test site. The term "calibrated" is used in this paper in the context of evaluating results of the exploratory methods against known well conditions. That is, are the exploratory methods identifying useful subsurface information for reservoir delineation?

The DVGW (also referred to as the calibration area herein) encompasses an area of approximately 170 km^2 and was part of a larger project area covering 2500 km^2 (Fig. 1). Much of the work presented herein has been published in the Geothermal Resources Council Transactions (Iovenitti et al., 2011), the Stanford Geothermal Engineering Workshop (Iovenitti et al., 2012, 2013) and the World Geothermal Congress (Iovenitti et al., 2015). It is re-presented in this special issue on EGS to provide an exploration perspective.

In the USA the total EGS resource base has been estimated by MIT (2006) at 13 million exajoules (3.6E + 15 MWh). The US Geological Survey (USGS) estimated the mean electric power resource for EGS on private and accessible public land in the USA as 517,800 MWe, with a 95% probability of 345,100 MWe and a 5% probability of 727,900 MWe (USGS, 2008). While there is agreement that the USA EGS resource is large, there is no widely accepted, invasive or non-invasive exploratory methodology for "greenfield" EGS sites proven to be both technically feasible and cost effective. Drilling slimholes to identify the actual resource base allows direct identification and measurement of the primary EGS resource critical geoscience parameters, described above, but widespread use of this methodology is cost prohibitive and as such, must be used selectively. The development of a cost effective and reliable exploration approach is essential for the economic viability of EGS in regions beyond those already explored for hydrothermal resources.

The DVGW was used as a calibration test site for development of an EGS exploration methodology because it has an extensive, public domain geoscience database along with well data consisting of lithology from 22 wells, bottomhole temperatures from 26 wells, temperature–depth data for 10 deep (productive and non-productive) wells and nine temperature gradient holes. This wellfield also has the highest bottomhole temperature for any published geothermal well in the B&R, 285 °C at 3000 m in well 36-14, in the Dixie Valley Power Partners (DVPP) portion of the field, WSW of the Dixie Valley Producing Field (DVPF), see Fig. 1. It also lies within the greater Dixie Valley Geothermal District, which is defined as a region encompassing multiple occurrences of geother-

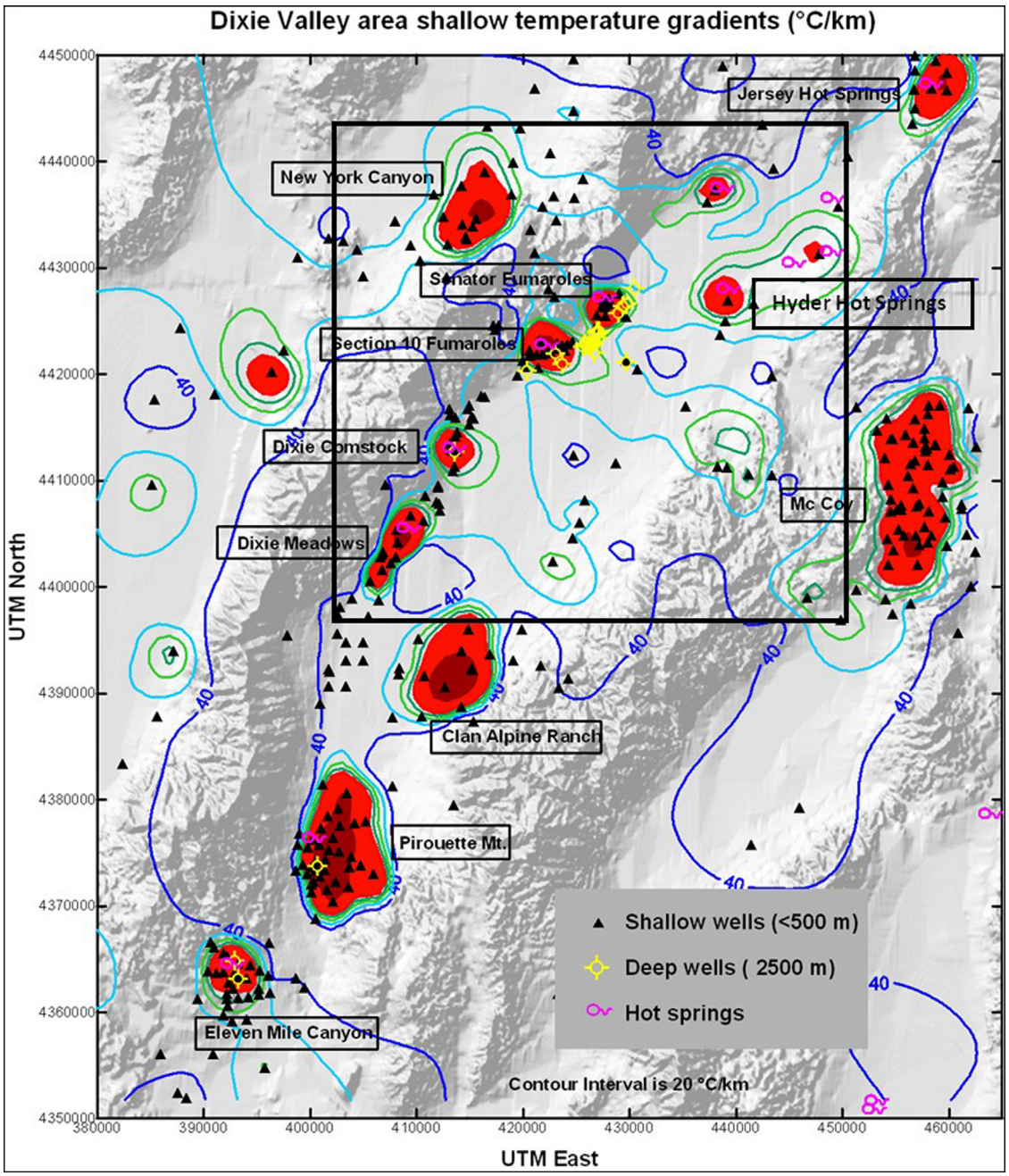

Fig. 2. Shallow thermal anomalies and shallow and deep well locations in the Dixie Valley Geothermal District. Temperature gradient contours in the ranges are diagrammatic and the contour intervals are 20 °C/km. From 120–250 °C/km the contours are a red fill and from 500 °C/km are a purple fill. Temperature gradient well locations are shown as black triangles for shallow wells (<~500 m) and yellow symbols indicate wells ≫500 m. Each red filled area in the Dixie Valley Geothermal District represents a separate geothermal cell/system. The project area is outlined by a black square. The figure and modified caption are after Blackwell et al. (2005, 2007). (For interpretation of the references to color in this figure legend, the reader is referred to the web version of this article.)

mal cells/systems (Fig. 2; Waibel, 1987, 2011; Iovenitti et al., 2011, 2012, 2015). The DVGW is producing 67 MW of electrical power using flash (62 MW since the early 1980s) and binary (5 MW bottoming cycle since January 2012) technologies.

This paper summarizes some of the work detailed in AltaRock Energy Inc. (2014a) on the Baseline Conceptual Model for the DVGW. It encompasses a comprehensive review of most of the work conducted on this geothermal system ca. 2011 and its reinterpretation.

2. Geologic setting

As reported by Blackwell et al. (2005), the Dixie Valley Geothermal System lies (1) within the Battle Mountain Heat Flow High (Mase and Sass, 1980), (2) at a major lithospheric boundary identified as the $^{87}Sr/^{86}Sr$ 0.706 line separating Mesozoic accreted terrains forming thinner crust and lower surface elevation to the W from Precambrian cratonal rocks forming thicker crust and higher surface elevation to the E (Wooden et al., 1999), (3) within the Central Nevada Seismic Belt, a zone of NNE-trending focused

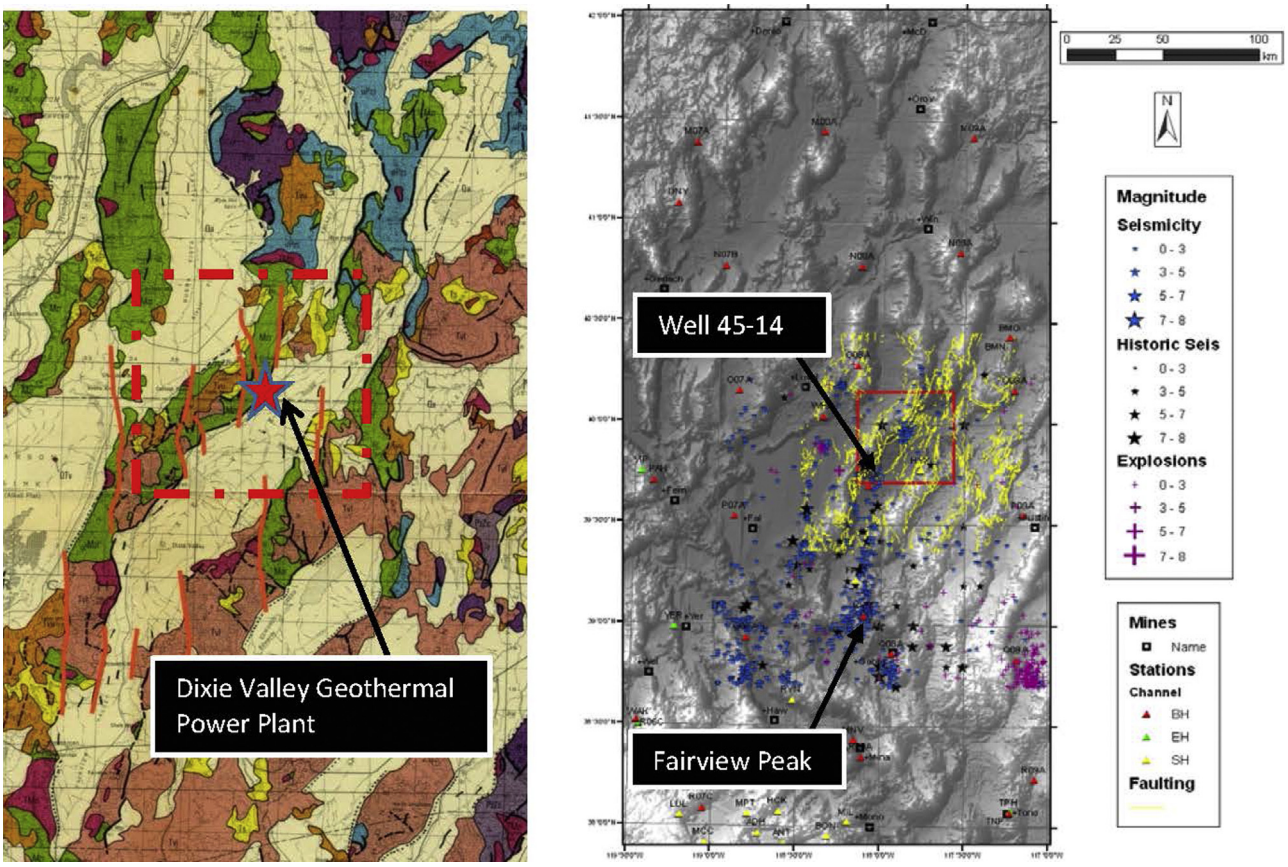

Fig. 3. N–S faulting in the project area (red dashed outline in both figures) as evidenced in the State of Nevada geologic map (Stewart and Carlson, 1978; left-hand figure) and re-interpreted natural and induced seismicity from 1900 to 2010 (right-hand figure) from AltaRock Energy Inc. (2014a), Iovenitti et al. (2011, 2015). Note that the Stewart and Carlson map is generalized and the reader is referred to Fig. 5 for the detailed structure of the project area. (For interpretation of the references to color in this figure legend, the reader is referred to the web version of this article.)

contemporary seismicity (Bell et al., 2004) and (4) in the lowest topographical valley in northern Nevada.

The regional stratigraphy of the area exposed in the Stillwater Range consists of allochthonous thrust plates of Triassic and Jurassic meta-sediments and Jurassic mafic igneous rocks that were intruded by late Cretaceous granodiorite and overlain by mid-Cenozoic volcanic rocks (Speed, 1976; Waibel, 1987). Within the adjacent Dixie Valley, the basement assemblage and overlying volcanics were in turn overlain by basin-fill sediments deposited during extensional events (Waibel, 1987).

The key structural elements for this study were created by two main extensional phases (1) pre-8 Ma B&R E–W extension expressed by a series of N-trending normal faults throughout the project area and (2) post-8 Ma to present B&R WNW–ESE extension expressed as NNE-trending normal faults (Waibel, 1987, 2011; Iovenitti et al., 2011). Both of these sets of structural features are evident in the state of Nevada geologic map (Stewart and Carlson, 1978) and the relocated natural and induced seismicity map for the greater Dixie Valley region for the period, 1900–2010 (Fig. 3).

The major range-bounding fault transecting the project area, the Dixie Valley Fault, is one of the most well-known normal faults in the B&R. It last ruptured at the surface during the 1954 Fairview Peak–Dixie Valley earthquake, M_S6.8 in Dixie Valley and M_S7.2 at Fairview Peak (Caskey et al., 1996). The DVPF (Fig. 1) lies within a zone referred to as the Stillwater Seismic Gap, which occurs S of the 1915 Pleasant Valley and N of the 1954 Fairview Peak ruptures (Wallace and Whitney, 1984; Caskey and Wesnousky, 2000).

Early structural models for Dixie Valley (Okaya and Thompson, 1985; Benoit, 1999) identified a single, moderately E-dipping (~54°) normal fault bounding the Stillwater Range on its eastern side and supported by surface fault measurements, interpretation of seismic reflection data. Issues with the dip of the fault were raised in Blackwell et al. (1999). Recent interpretations based on wellfield, gravity, and magnetic data defined a much more complex, multi-fault setting referred to as the Dixie Valley Fault Zone (DVFZ) within the area of the wellfield. The DVFZ is a complex and steeply dipping structure (~75–80°) consisting of the range-front fault (referred to as either the Dixie Valley Fault (Benoit, 1999) or the Stillwater Fault (Hickman et al., 1998, 2000), and at least one major piedmont fault, which is not continuously expressed at the surface, but accounts for the majority of displacement between the range and the valley (Smith et al., 2001, 2002; Blackwell et al., 2002, 2005). Gravity and magnetic (2.5D joint inversion) modeling (Iovenitti et al., 2015; AltaRock Energy Inc., 2014a) confirmed the complex DVFZ.

3. Study results

Using the existing public domain data, a baseline conceptual geothermal model was developed (Iovenitti et al., 2012; AltaRock Energy Inc., 2014a) and qualitative correlations between various geoscience data sets were determined and cross-correlated with known well results. Described below are the generalized stratigraphy of the project area, structural setting findings, major qualitative correlations, quantitative geostatistical analysis, and the paired EGS favorability and trust maps.

3.1. Stratigraphy

The stratigraphy in the project area was generalized into eight formations (seven major and one minor) based on their field occurrence and their potential to host an EGS and/or a hydrothermal reservoir (Fig. 4). In Dixie Valley the hydrothermal reservoir currently being exploited is principally a fault/fracture system.

3.2. Structural findings

The baseline conceptual structural model is presented in Fig. 5. The data sets used to derive the structure map include mapping results from Page (1965) and Speed (1976), structures identified by Smith et al. (2001) and geophysically inferred structures including horizontal gravity gradients (Blackwell et al., 2005), faults recognized by the state of Nevada and from the USGS Quaternary Fault and Fold Database, and relocated seismic events in the last century indicating N-trending faults, specifically along a major active structure extending from Fairview Peak and continuing into the Project Area due W of well 45-14 (Iovenitti et al., 2011). Fig. 5 also represents the compilation and re-interpreted relationships of all known faults and inferred structures in the project area along with the shallow thermal anomalies (at $\ll$500 m depth) in the area. The structures are all assumed to be steeply dipping with dip directions derived from stratigraphic relationships, surface measurements and geophysics.

Analysis of the overall structural setting of the project area reveals that the intersection of the pre-8 Ma N-trending B&R structures (Waibel, 1987) with the current NE-trending post-8 Ma B&R structures are coincident with the location of the shallow thermal anomalies along both sides of the Stillwater Range (Iovenitti et al., 2011, 2012, 2015). In some cases, the older N-trending structures appear to offset NE oriented structures within the DVFZ suggesting re-activation within the current stress regime.

The structural zones at these major fault intersections were divided into compressional and dilatational areas based on the expected movement within discrete structural blocks in their respective quadrants (Fig. 5). The model assumes the NE-trending normal faults exhibit pure normal slip, with slip vectors perpendicular from fault strike. For the N-trending faults, the major assumption is the faults exhibit strike–slip motion under the current stress regime. This same type of motion was also reported by Caskey et al. (1996) on the Fairview Peak 1954 earthquake. The zones of compression and dilatation were derived from the combination of expected slip (direction) on a NE-trending fault and the expected strike-slip component on N-trending faults. Where both vectors agree (in same directions) a zone of dilatation[1] is inferred. Where the vectors diverge, a zone of compression is inferred, as movement on the strike–slip fault dominates. Also an abrupt bend in a normal fault, apparent as the piedmont fault takes a significant left-step bend in the producing field, would also infer a dilated zone at the change in strike of the fault. The extent of these compressional and dilatational areas is purely arbitrary and is assumed to extend about a kilometer away from the intersection. The structural and thermal data indicate that these structural intersections play an important role in the development of the shallow thermal anomalies given their spatial coincidence and expectedly host various geothermal cells/systems within the overall Dixie Valley Geothermal District (Figs. 2 and 5).

AltaRock Energy Inc. (2014a) and Iovenitti et al. (2012, 2015) described correlations between various structural zone types (compression, dilation, or other) with the helium R/Ra values for fumaroles and hot springs (Kennedy and van Soest, 2006) and different well types (e.g., producer, sub-commercial well, non-producer) for the DVGW. In summary, all available producers to the studies reported occur in a dilated zone and these wells show a slightly elevated magmatic signature (Kennedy and van Soest (2006). All available injectors to this study occur in dilation or "other" structural zones. Most available non-producer/sub-commercial wells occur in compression and/or "other" structural zones. These data coupled with the spatial coincidence of some of the shallow thermal anomalies in the Dixie Valley Geothermal District with the structural intersection of N-trending and NE-trending faults strongly implies that the identified dilated zones (Fig. 5) extend from the surface to the depth of the hydrothermal reservoir currently being produced.

3.3. Role of lithology in the geothermal system

Rock type at elevated temperature also plays a significant role in whether a well is a producer or non-producer in a hydrothermal system and whether a non-producing conventional well can be stimulated to host an EGS reservoir. Current geothermal electrical production is derived from the piedmont fault component of the DVFZ (Blackwell et al., 2005) at structural intersections described above. The geothermal reservoir lies within brittle igneous rocks including Miocene basalt and Jurassic mafic rocks that are juxtaposed against impermeable granodiorite along a steeply dipping structure (Lutz et al., 1997; Benoit, 1999; Blackwell et al., 2005; Reed, 2007). Brittle rocks containing open fractures are an ideal hydrothermal reservoir. When closed fractures are present in such brittle rocks, the rock can be hydrosheared to form an EGS. Non-brittle rocks would not be appropriate for either a hydrothermal system or an EGS. Several examples of wells completed in poor reservoir rock exist within the DVGW. The non-producers 45-14 and 66-21 located in the southwestern portion of the DVGW have bottomhole temperatures of 196 °C and 215 °C, respectively, but were completed in Triassic shales, not a suitable reservoir rock (D. Benoit, pers. comm., 2011). This is the case because it appears that the Triassic shales in the areas drilled do not sustain fractures. The northernmost producing wells, 27-33, 28-33, and 37-33, all lie within a dilated zone, while an adjacent dry hole, 82-5, lies with a zone of compression separating the aforementioned wells from the main production area to the SW. Hickman et al. (2000) also reported that 82-5 is completed in a narrowly defined shear zone with abundant talc alteration and low shear stress at the depth where the well was expected to encounter the producing fault zone.

3.4. Qualitative geoscience correlations

Six detailed geoscience cross-sections (perpendicular and parallel to the DVFZ) through the DVGW were constructed (Fig. 6) based on public domain well data, surface and subsurface geology, available interpreted seismic reflection profiles and geophysical surveys that inferred structures within Dixie Valley. Plate 1 presents these sections C-C′ to F-F′ (C–F) perpendicular to the range-front fault. The geologic and thermal sections provided a basis for a correlation analysis that compared the sections with various geophysical models including magnetotellurics (MT), 2½-D gravity/magnetics, and seismic velocity models. These sections are presented in a serial view looking N45°E approximately parallel to the range front fault.

An analysis of the degree of correlation between data depicted along sections (C–F) in Plate 1 was performed. Details of this correlation are provided in AltaRock Energy Inc. (2014a). Findings along two sections, C-C′ and E-E′, are described in detail in Iovenitti et al. (2011) and Iovenitti et al. (2012), respectively. The latter is re-produced, in part, herein for the purposes of this article.

[1] The terms dilation and dilatation and their derivatives are used interchangeably in this text.

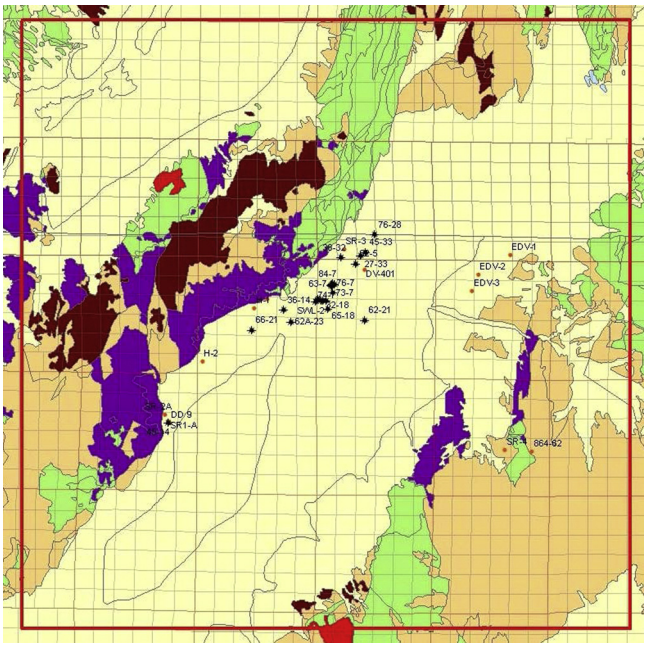

Fig. 4. Generalized stratigraphy in the project area (red outline) adapted from Speed (1976). From oldest to youngest the project area formations are (1) Paleozoic meta-sediments (Pz, blue), (2) Triassic meta-sediments (Tr, green), (3) Jurassic mafic rocks also referred to as the Humboldt Igneous Group and the Humboldt Lopolith (Jz, purple), (4) Jurassic Boyer Ranch quartzite (Jbr, a minor formation not shown at this scale), (5) Cretaceous granodiorite (Kgr, red), (6) Oligocene silicic volcanics (Tv, orange), (7) Miocene basalt (Tmb, brown) and (8) late-Cenozoic basin-filling sediments (QTbf, yellow). Geothermal wells (>1000 m) and temperature gradient holes (300–1000 m) are shown in black well symbols and as red dots, respectively. The small squares are 1 mile or 1.61 km on a side. (For interpretation of the references to color in this figure legend, the reader is referred to the web version of this article.)

Fig. 7 presents the correlation in the geology, MT, thermal (temperature) and gravity-magnetics lithology-structural model along sections E-E′. Note that the p-wave velocity model is not discussed herein due to its poor correlation with the geology sections (Plate 1). In section E-E′ as well as the other sections in Plate 1, the geology section is superimposed on the MT and the thermal sections. Similarly, the thermal section is superimposed on the geology and MT sections. Generalized geothermal well trajectories along a section line or in the immediate vicinity of the section line are also indicated. It should also be noted that the temperature distribution along all the sections in Plate 1 is primarily determined by the temperature data available from wells along and in the vicinity of the section and secondarily by the temperature distribution on surrounding sections to the NE and SW.

The generalized geology section E-E′ indicates the presence of the DVFZ based on surface geology, well data and geophysical data such as the MT, gravity/magnetics model, and to a lesser extent the seismic reflection profile (in Plate 1). Important observations along section E-E′ are (1) the presence of a steeply dipping low resistivity structure, roughly parallel to the range-front fault but on the footwall side, that correlates with known areas of intra-range faulting, (2) a relatively higher resistivity block associated with the geothermal reservoir in the area of the production wells in the hanging wall of the piedmont fault element of the DVFZ, (3) the correspondence of the gravity–magnetic inferred lithology model with the interpreted geologic section, specifically the occurrence of the Jurassic section (Jz) defined as magnetic Jurassic mafic rocks (Jg), (4) missing Jg in the valley coincident with the major low resistivity zone to depth as reported by Wannamaker et al. (2006, 2007) which is interpreted to reflect demagnetized Jg possibly attributed to hydrothermal alteration, (5) thermal upflow along both the range-front and piedmont faults in the DVFZ and (6) high resistivity in the Stillwater Range is not observed until about the center of the range and is interpreted as unaltered granodiorite (Kgr). The resistivity distribution under the Stillwater Range along section E-E′ suggests the presence of a hydrothermal cell in the footwall of a range-front fault component of the DVFZ in this area. Note that the dip of the faults shown on the gravity–magnetic sections is approximate and the modeled structure can easily accommodate changes in dip comparable to those shown in the geology sections.

Major correlations found throughout the sections C–F (Plate 1) are (1) MT profiles show a high level of correlation with the interpreted structure in the geologic sections; (2) a vertical-trending low resistivity zone seen in the three MT profiles within the valley may in part reflect a major alteration zone correlating with a set of N-trending structures; (3) the gravity/magnetic profiles reflect the interpreted generalized geology, and show that the magnetic signature of the Jurassic mafic rocks does not extend through this major N-trending intra-valley structure and is locally not present within the DVFZ; and (4) the areas of elevated temperature occur at the intersection of the N-trending faults and NE-trending segments of the piedmont fault. Additional details of these correlations can be visually found in Plate 1 and in Iovenitti et al. (2011, 2012, 2015).

4. Quantitative geostatistical analysis

Exploratory geostatistical data analysis was applied to the following geoscience parameters: fracture intensity, lithology density, vertical stress, Coulomb Stress Change (CSC), dilatation strain (derived from the Coulomb Stress Change model), temperature, p-wave velocity (Vp) and MT resistivity. The available data sets that have varying resolution were either measured, modeled/calculated or inferred and gridded along the section lines within the 0.5 km × 0.5 km cells (see Fig. 7) to provide a consistent grid size for statistical analysis. Analyses conducted with the aforementioned geoscience parameters were (1) global (undivided per categorical groups such as different formations) linear correlations along sections C-C′ through F-F′; (2) multivariate analysis of various geoscience parameters with lithology per sections C-C′ through F-F′; (3) global domain analysis that divides the sectional

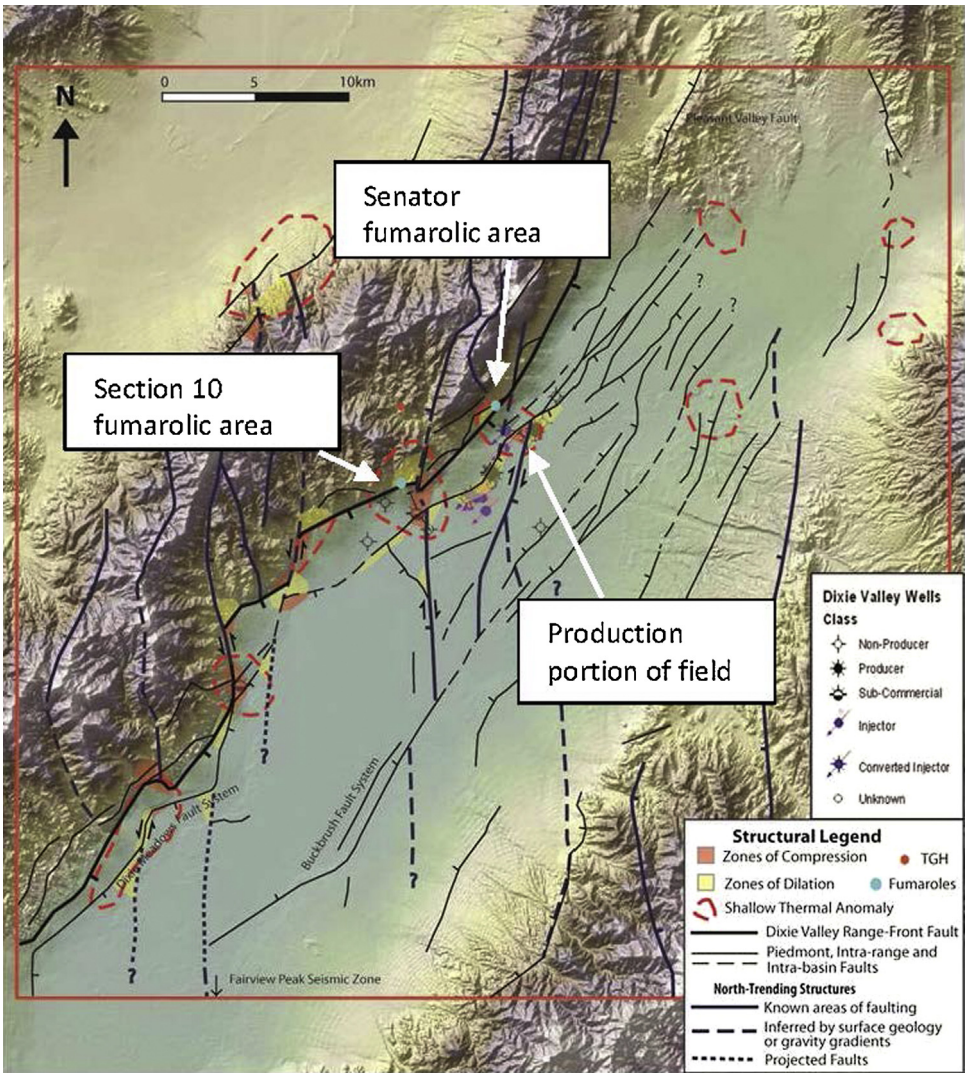

Fig. 5. Correlation between shallow thermal anomalies (dashed red lines) and identified structural intersections of N- to NE-trending faults (black lines) in northern Dixie Valley, Nevada. Production area is in the northern portion of the field. Blue dots indicate the Section 10 and Senator fumarolic areas. Black dots indicate deep wells, while red dots indicate relatively deep (1500 m) temperature gradient holes. Expected zones of compression (orange shaded areas) and dilation (yellow shaded areas) occurring at the intersections of discrete structural blocks are also shown. The figure and caption are from Iovenitti et al. (2012). (For interpretation of the references to color in this figure legend, the reader is referred to the web version of this article.)

data into three domains: Stillwater Range, DVFZ and the valley; (4) global domain analysis of the three domains mentioned using well data only; (5) ChiSquare test on the gravity–magnetic models and geologic models; (6) Classification and Regression Tree (CART) using temperature, *Vp*, resistivity (MT), CSC, dilatation, fault presence, vertical stress, lithology relative to the section data and the well data.

The purpose of the geostatistical analysis was to, among other factors, (1) quantify the qualitative geoscience correlations, (2) investigate the suggestion by Biasi et al. (2008) that seismic data correlates with temperature and rock type, (3) determine the predictive power of various geoscience parameters for rock type and temperature, and (4) assist in the data generation for the EGS favorability/trust maps. Details of this work are provided in AltaRock Energy Inc. (2014a,b), Iovenitti et al. (2011, 2012, 2013). It should be noted that the geostatistical data was not used in the generation of the EGS favorability/trust maps, described below. This resulted from the case that the measured, modeled and inferred data was considered more appropriate for the purposes of calibrating the exploration methodology than using the geostatistical data in the construction of the aforementioned maps. To see if this exploration approach would be viable without having extensive subsurface temperature data, we evaluated whether the baseline dataset could be used to predict any or all of the key EGS identified parameters of temperature, lithology and stress without the measured temperature data from the wells: this is presented below.

A multiple regression analysis using Statistical Analysis Software (SAS) of temperature vs. key geoscience parameters including elevation, vertical stress, dilatation, *Vp*, and resistivity using the sectional data was also performed. This multicomponent analysis indicated that (1) the combination of a variety of geoscience parameters could predict temperature with an r^2-value of 0.94 (Fig. 8a), and (2) there is a complex interaction between the geoscience parameters in this prediction (Fig. 8b). In the DVGW, it is known by measured temperatures in the wells available to this study that temperatures increase with depth and vertical stress increases with depth. Attempts were made to remove this effect by examining temperature residuals and a poor correlation was found. As such, no further consideration of this approach was made in AltaRock Energy Inc. (2014a,b). However, the CART analysis did provide interesting correlations (AltaRock Energy Inc., 2014a; Iovenitti et al., 2011,

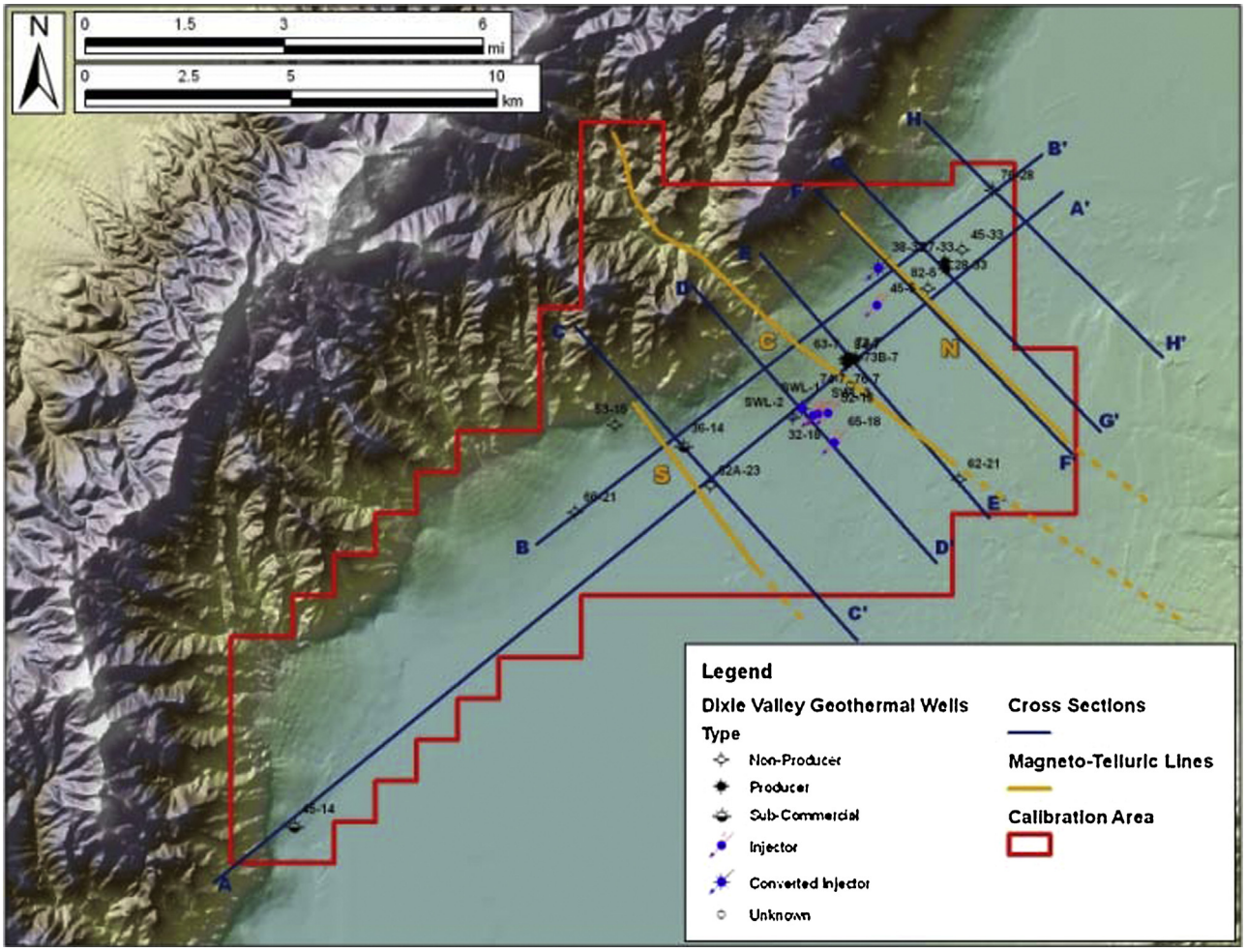

Fig. 6. The Dixie Valley Geothermal Wellfield. Location of cross-section lines C-C′ through H-H′) and MT arrays N, C, and S from Wannamaker et al. (2006, 2007) presented in Plate 1 are shown as blue and orange lines, respectively. (For interpretation of the references to color in this figure legend, the reader is referred to the web version of this article.)

2012, 2013) with respect to the aforementioned inquiry and these are discussed below.

CART is a statistical method that can be used to determine the relationship between response variables (RVs, i.e., the parameter to be predicted, e.g., temperature), and multiple explanatory variables (EVs, the geoscience parameters defined above which are not being predicted). Lawrence and Wright (2001) reported that CART operates by recursively splitting the data until ending points, or terminal nodes, are achieved using preset criteria by analyzing all EVs and determining which binary divisions of a single EV best reduces deviance in the RV. For each portion of the data that results from this split, the process is repeated, and continues for categorical data until homogeneous terminal nodes are reached in a hierarchical tree. In our case where numerical data is used, the split process was repeated until cross-validation determined that the deviance was no longer decreasing appreciably and thus, no more splits should be made.

Decision trees in CART are designed to quantify the amount of variability (i.e., r^2-value) in the RV that can be explained by the EVs available to make the prediction. Classification trees predict what category a categorical RV falls into whereas regression trees predict a numerical RV's value. For a categorical variable, EVs are used to determine split points that are chosen to minimize the number of misclassifications (technically to minimize Gini impurity). For more than two categories (e.g., two geologic formations at Dixie Valley) for any EV this is equivalent to choosing the split points so that a random grid cell has the smallest possible chance of being misclassified. Thus if we have i categories, each with probability pi, we minimize the sum of pi(1 − pi), summed over the i categories in each of the branches at the end of the splits. If the categories are all perfectly classified, pi will be 1 for exactly one value of i and then (1 − pi) will be 0 for that category. In construction of a regression tree to predict the numerical value of a RV, the process of splitting is done to minimize the squared errors of the predictions when the predictions are the averages within the subgroups. If the splitting is allowed to continue, it will have the undesirable effect of fitting noise. Because of this, pruning methods such as cross validation are used to reduce the tree in a way that presents an accurate realization of how the predictions should be applied to data not included in the building of the tree. Amongst the advantages of CART are that it results in easily understandable prediction rules and it is free of underlying assumptions about the data and data error structure (e.g., MT resistivity model). Drawbacks include that it is restricted by binary splits and since the optimization is done from the top down it may not result in the globally optimal tree.

CART was used to examine select input parameters (EVs) to predict the following RVs (1) temperature, (2) lithology, (3) productive vs. non-productive hydrothermal cells and (4) expected EGS favorable cells using both section and well data. Note that we examined productive vs. non-productive hydrothermal cells in this analysis since a holistic treatment of the DVGW was conducted in this EGS study. The term cell refers to the gridding scheme (0.5 km × 0.5 km)

Table 1
Classification and Regression Tree (CART) Sensitivity Analysis results using section and well data. The first row for each response variable corresponds to r^2-value ranges with vertical stress considered, while the following rows, highlighted in green, show the r^2-values when vertical stress is removed from the analysis. In most cases with the exception of predicting lithology using section data, a similar r^2 result can be achieved when vertical stress is removed from analysis. See text for explanatory variables used in this analysis. The caption and table are after Iovenitti et al. (2013).

Response Variable Prediction	Data Type	Explanatory Variables Removed from Analysis							Explanatory Variables in the Analysis Used when Vertical Stress Is Removed
		0	1	2	3	4	5	6	
Temperature	Section		.729 - .918	.727 - .918	.847 - .907	.735 - .898	.310 - .901	0.874	
Temperature (Vertical Stress is removed from consideration)		0.871	0.677						Vp, Resistivity (MT) and Gravity-Magnetic (G-M) Lithology
				0.810					Resistivity (MT), CSC, Dilatation and Lithology
					0.792				Vp, Resistivity (MT) and Dilatation
						0.885			Vp, Dilatation and Lithology
							0.775		Vp and Resistivity (MT)
								0.684	Dilatation
Lithology			.627 - .655	.541 - .655	.523 - .665	.484 - .660	.505 - .656	0.507	
Lithology (Vertical Stress is removed from consideration)		0.631	0.438						Vp, Resistivity (MT), Dilatation and G-M Lithology
				0.453					Vp, Resistivity (MT), Dilatation and Temperature
					0.433				Vp, Resistivity (MT), Dilatatio and G-M Lithology
						0.421			Vp, Dilatation and G-M Lithology
							0.406		Vp, and Dilatation
								0.277	Dilatation
Temperature	Well		.769- .841	.749- .841	.749 - .822	.749 - .805	.749 - .803	0.749	
Temperature (Vertical Stress is removed from consideration)		0.841	0.750						Vp, Resistivity (MT), CSC, Dilatation and Lithology
				0.767					Vp, Resistivity (MT), CSC, Dilatation and G-M Lithology
					0.775				Vp, CSC, Dilatation and G-M Lithology
						0.730			Vp, Dilatation and Lithology
							0.680		Vp and Lithology
								0.621	Vp
Lithology			.577 - .611	.562 - .611	.562 - .644	.562 - .620	.552 - .615	0.552	
Lithology (Vertical Stress is removed from consideration)		0.611	0.521						Vp, Resistivity (MT), CSC and G-M Lithology
				0.529					Vp, Resistivity (MT), CSC and G-M Lithology
					0.600				Vp, CSC and G-M Lithology
						0.550			Vp, CSC and G-M Lithology
						0.549			Vp, Dilatation and Temperature
							0.550		Vp and Dilatation
								0.408	Vp
Productive vs. Non-productive cells			.447 - .617	.431 - .663	.523 - .665	.437 - .648	.315 - .587	0.389	
Productive vs. Non-productive Cells (Vertical Stress is removed from consideration)		0.625	0.528						Vp, Resistivity (MT) and Lithology
				0.615					Vp, Resistivity (MT), Lithology and Dilatation
					0.416				Vp, Resistivity (MT), Dilatation and G-M Lithology
					0.416				Vp, Dilatation, G-M Lithlogy
						0.598			Vp, Lithology and Dilatation
							0.550		Vp and Lithology
								0.457	Lithology
Expected EGS favorable cells			.523 - .727	.409 - .727	.383 - .727	.369 - .727	.34 - .727	.34 - .637	
EGS favorable cells (Vertical Stress is removed from consideration)		0.708	0.708						Temperature, Vp, CSC, Dilatation, Resistivity (MT), Fault and Lithology
				0.769					Temperature, Vp, CSC, Dilatation, Resistivity (MT) and Fault
					0.769				Temperature, Vp,, Resistivity (MT), CSC and Dilatation
					0.769				Temperature, Dilatation, an dG-M Lithology
						0.769			Temperature, Vp, CSC and Dilatation
							0.708		Temperature, Dilatation and Lithology
								0.708	Dilatation and Lithology

Table 2
EGS favorability mapping parameters, temperature, lithology and stress sub-parameters (shaded green). Their values range from 1 to 9 (shaded yellow). The parameter weights sum to 1.

Temp[1] (0.50w[2])		Lithology[3] (0.30w)		Stress sub-parameters (0.20w)							
				Compression / Dilatation Zone (0.05w)		*Fault Orientation (0.50w)*		*Structure Present (0.50w)*		*Coulomb Stress Change (0.05w)*	
100	1	QTbf	1	Compression	4	30-60°	7	Structure	7	<-22	22
125	2	Tmb	5	Dilatation	7	Other	4	None	5	-22	3
150	3	Jz	7	Neither	5	Neither	5			-14	3
175	4	Tr	3							-6	4
200	7	Kgr	9							0	5
225	7	Tv	3							6	6
250	8	Jbr	8							14	7
275	9									22	8
300	8									>22	9
325	7										
350	5										
>374	3										

[1]Temperature (°C).
[2]Parameter weight.
[3]Generalized formations in Dixie Valley; see Fig. 4.

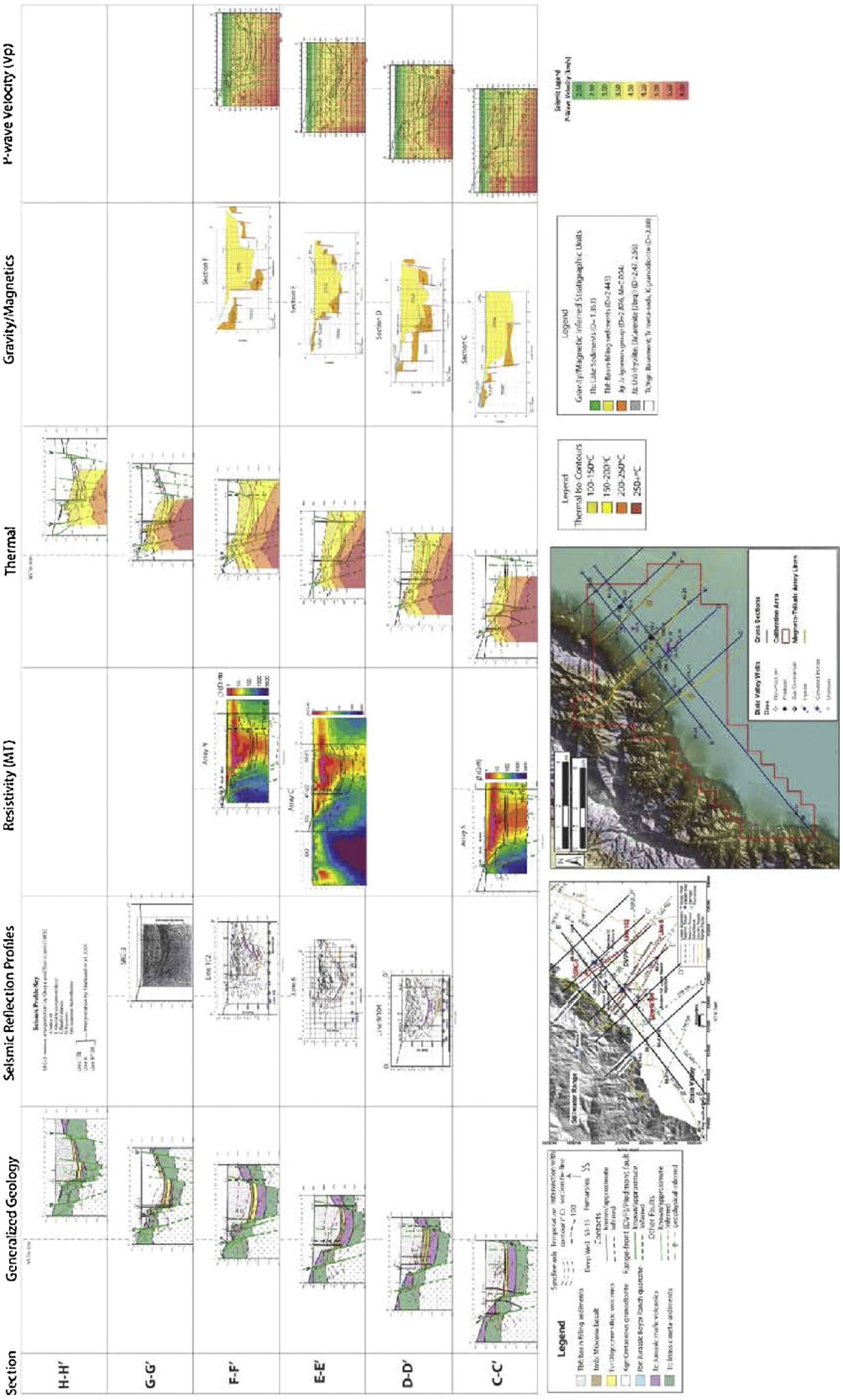

Plate 1. Correlation of Sections perpendicular to the Dixie Valley Fault Zone.

used in assessing the geostatistical significance of the various geoscience EVs considered. Table 1 presents the results of this analysis using the EVs (1) temperature, (2) p-wave velocity (*Vp*), (3) resistivity from MT, (4) Coulomb Stress Change (CSC) and (5) dilatational strain (dilatation) both from Coulomb Stress modeling, (6) with and without vertical stress for reasons described above and below, (7)

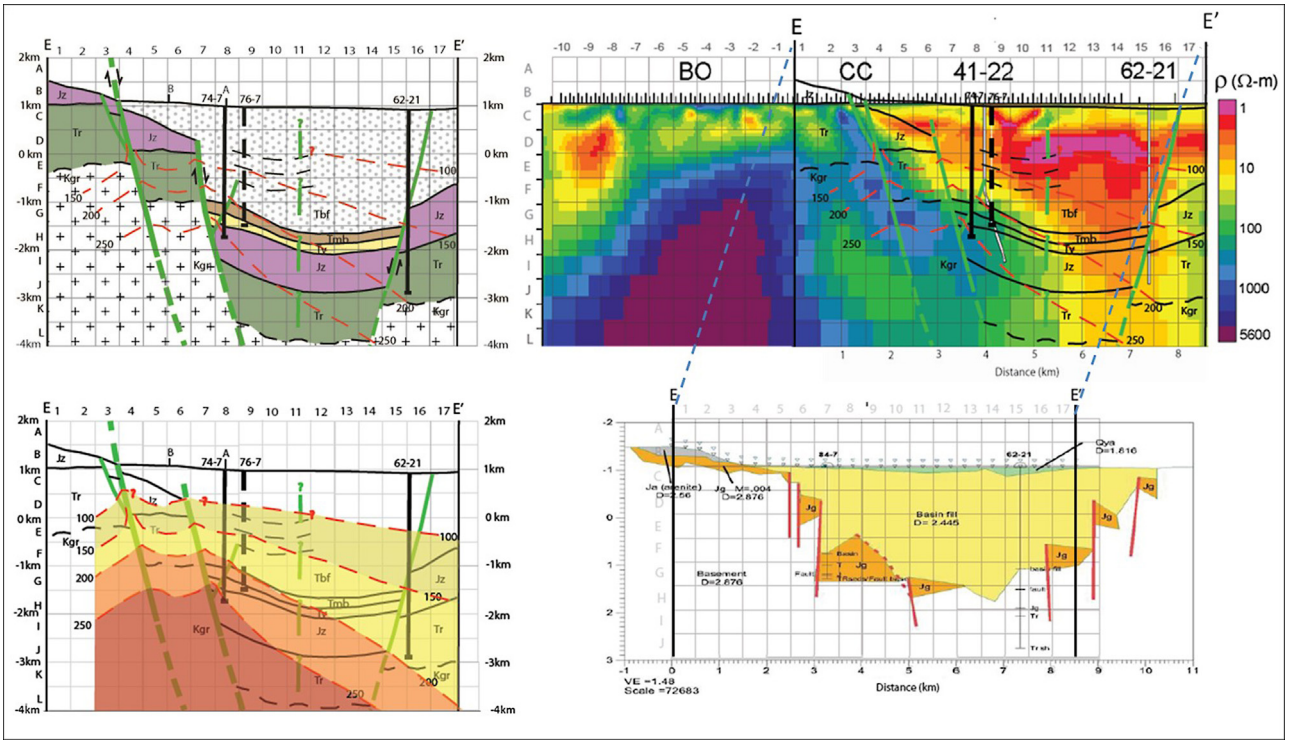

Fig. 7. Correlation of the geology (upper left), magnetotelluric resistivity (MT, upper right), thermal (lower right) and gravity–magnetic lithologic-structure model (lower right) along Section E-E′; see Fig. 6 and Plate 1 for location. Generalized geothermal well trajectories are shown in the geology, MT and thermal sections. The thermal section is superimposed on the geology and MT sections. The geology section is superimposed on the MT and thermal sections. The gravity–magnetic has no additional sections superimposed on it for the sake of clarity. A 0.5 km × 0.5 km grid is superimposed on all sections for correlation purposes as well as for geostatistical and EGS favorability/trust mapping; see text. A generalized hot spring (S) location is shown on the geology section. The extension of the fault in grid B3 is for fault motion purposes only. Geothermal wells along the section are shown as dark black lines and wells projected on the section are indicated by the dashed black lines. Well IDs are indicated. Temperatures isotherms are depicted as dashed red lines. See text for a description of the geologic formations (e.g., Kgr). (For interpretation of the references to color in this figure legend, the reader is referred to the web version of this article.)

lithologic formations derived from the geologic assessment and (8) lithology from the coupled gravity–magnetic modeling.

Table 1 displays the range of r^2-values resulting from the CART analyses that explored all combinations of the EVs used in the analysis for predicting (1) temperature and lithology using section and well data, (2) temperature, lithology, productive (hydrothermal) vs. non-productive cells and expected EGS cells using well data. It was recognized in the preliminary analysis (AltaRock Energy Inc., 2014a; Iovenitti et al., 2012) that while high r^2-values were determined for the vast majority of the CART predictions, vertical stress, considered a surrogate for depth, was the most likely EV to split on. Thus, the consideration that this parameter could produce artificially high r^2-value results for the CART predictions developed. As such, we conducted a CART sensitivity analysis to explicitly remove the vertical stress parameter as well as determined what set of EVs could be used to predict the RVs with any precision. It should be noted that in a CART analysis there is a difference between the parameters considered in the analysis and those actually used in the analysis. The explanatory variables used in the analyses include a variable combination of (1) temperature, (2) p-wave velocity (*Vp*), (3) resistivity from MT, (4) CSC and (5) dilatational strain (dilatation) from Coulomb Stress modeling, (6) vertical stress, (7) lithology from geology, (8) lithology from joint gravity–magnetic modeling and (9) the presence or absence of a fault.

The r^2-value ranges with all EVs considered (i.e., vertical stress included) are reported in the first row in Table 1 for each RV and shaded in white. Selective CART sensitivity results without the use of vertical stress are shown as green shaded cells. For the RVs of temperature and lithology and considering all the EVs, r^2-values of 0.871 and 0.631 were calculated using cross-section

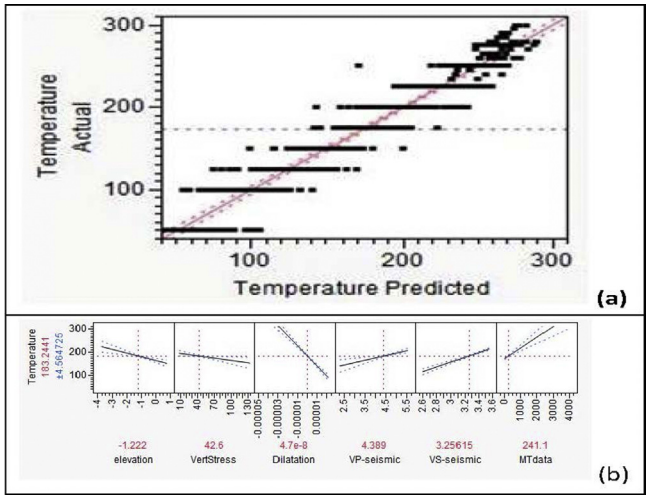

Fig. 8. (a) Actual (measured) temperature vs. predicted temperature using the following variables: elevation, resistivity, vertical stress, dilation, *Vp*, and *Vs* (S-wave velocity). The r^2-value for this analysis is 0.94. (b) Example of a Predictor Profile showing the complex interactions of the indicated parameters in predicting temperature. The figure and caption are from Iovenitti et al. (2012).

data only and removing the EV vertical stress from consideration, the highest r^2-values were 0.885 using only the EVs *Vp*, dilatation and lithology and 0.453 using the EVs *Vp*, resistivity, dilatation, and G–M lithology, respectively. Using well data only to predict the RVs temperature, lithology, productive vs. non-productive hydrothermal cells and expected EGS favorable cells, the calcu-

lated r^2-values, considering all the EVs, were 0.841, 0.611, 0.625 and 0.708, respectively. Removing the EV vertical stress from consideration, the highest r^2-values were 0.767 using the EVs *Vp*, resistivity, CSC, dilatation, and G–M lithology; 0.600 using the EVs *Vp*, CSC and lithology; 0.615 using the EVs *Vp*, resistivity, lithology and dilatation; 0.769 using the EVs temperature, *Vp*, CSC, dilatation, resistivity, fault and lithology; temperature, *Vp*, resistivity, CSC and dilatation; temperature, dilatation and G–M lithology; and temperature, *Vp*, resistivity, CSC and dilatation; depending on the number of EVs removed from consideration, respectively. These CART results, while intriguing, were not used in the generation of the favorability maps because this is the first analysis of its kind that the authors are aware of that has been applied to geothermal systems and more testing at other sites needs to be done; the raw total baseline data set described above was considered the most appropriate for this study. Additionally, it is debatable whether dilatation should be used to predict EGS favorability since this study showed that structural dilatation zones are directly associated with the shallow thermal anomalies and the deep geothermal production and injection wells and as such is a predictor of the presence of a hydrothermal reservoir. In this study the project team (see Acknowledgements section) decided to also include dilatation in the prediction for a viable EGS area.

Thus, CART analysis may be a viable method to be used to predict EGS favorability. However, it must be noted however that this is the first such use of this type of analysis that the authors are aware. The methodology should be tested at other sites to determine the full utility of the approach.

To complete the discussion of predicting EGS favorability using geoscience data, stress conditions must be considered. In this study, stress was predicted based on CSC modeling. One of the limitations of this approach is that it can only predict the stress changes on a receiver fault due to slip on a source fault with simplistic geometry and slip distribution. However, new modeling methodologies for predicting subsurface stress conditions considering shear stress release on detailed geometries of mapped surface and subsurface faults such as Poly 3D (Swyer and Davatzes, 2013) and a newly developed workflow that combines the use of the material point method and continuous fracture modeling (Aimene and Ouenes, 2015) could be used to develop greater insight on predicted subsurface stresses in a more holistic manner.

5. EGS favorability/trust maps

To identify favorable areas for EGS in the DVGW, EGS favorability/trust maps were made at a grid cell scale of 0.5 km by 0.5 km for 0.5 km incremental horizontal slices between +1 km asl and −4 km asl. The three parameters considered most important for EGS were mapped. These parameters, in order of importance, are temperature (above 200 °C but less than 350 °C), rock type (resistant, competent rock that can form fractures), and stress (extension being more favorable than compression). Since Dixie Valley is located in the B&R, a region of overall extension, we defined four stress sub-parameters to be considered in the favorability/trust analysis (1) fault orientation, (2) presence or absence of a fault, (3) CSC (see AltaRock Energy Inc., 2014a), and (4) occurrence of a structural zone including compression, dilatation, or neither. Subject Matter Experts (SMEs) on the project team (see Acknowledgements section) were polled to determine the relative favorability values of the individual parameters being considered as well as the final weighting to calculate overall EGS favorability. Weights for temperature, lithology and stress parameters are 0.50, 0.30 and 0.20, respectively. Table 2 presents the favorability weights and values used. Favorability values were calculated as follows:

$$F_v = (d_0 \times w_0) + (d_1 \times w_1) + \ldots (d_n \times w_n)$$

where F_v is the favorability value for a grid cell, d_0 through d_n is the favorability value of an individual cell's geoscience parameter data, and w is the weight for a particular data set. EGS favorability maps were calculated using an Excel spreadsheet and visualized using GIS software (ArcGIS 10). It should be noted that these maps represent one potential realization of the data, albeit, the best one from the author's point of view. A stochastic treatment of the data was not conducted.

Additionally, trust maps were also developed to complement the favorability map and they depict the reliability of the underlying data. Trust weights range from: hard data (i.e., from wells) with a weight of 5 to modeled and inferred data with weights ranging from 4 to 2, respectively, depending on SME confidence in the data, to no data with a weight of 1. The significance of the trust maps has been described in preceding sections. Fig. 9 presents the coupled favorability/trust maps for −1 km asl and −2.5 km asl. Note that these maps do not account for the presence of non-magnetic Jz rocks observed in the gravity–magnetic models (Plate 1).

6. Conclusions

A geothermal conceptual model using existing public domain data (ca. 2011) was developed for the DVGW. Important results from the assessment are the (1) marked correlation between the location of shallow thermal anomalies along both sides of the Stillwater Range front and the intersection of N-trending faults with NE-trending faults in the DVFZ, (2) presence of dilatation and compression zones at these structural intersections, (3) the cross-correlation of production, injection, and dry wells with both the structural zone type in which the well is located and the well's helium R/Ra values, (4) MT supporting data to the identification of the DVFZ postulated by Blackwell et al. (2005) and (6) evidence for the presence of dilatation zone that extend from the near subsurface to reservoir depths.

Qualitatively, there exists a very good correlation among the different geoscience data analyzed. The conceptual model was found to be applicable to both to the EGS and hydrothermal components in the DVGW.

Identification of brittle rocks capable of bearing fractures at depth is critical to development of an EGS. The Triassic metasediments in the DVGW, although hot, were not considered viable potential EGS reservoir rocks because they appear to not be able to sustain open fractures.

In addition to qualitative geoscience correlations, quantitative geostatistical analyses are reported which suggest that consideration of various geoscience parameters may be used to predict lithology, temperature, productive vs. non-productive hydrothermal cells and expected EGS favorable cells.

EGS favorability/trust maps were constructed deterministically by the project SMEs. Potential areas of EGS interest were identified based on an integrated assessment of the three EGS parameters of interest: temperature, lithology and stress, (i.e., favorability map) and the reliability of the underlying data defined using complimentary trust maps. The areas shown in red on the favorability maps presented are most favorable for locating EGS at the depth indicated. The complimentary trust map for a given depth reflects the confidence in the data used in creating the favorability map.

The coupled Dixie Valley Geothermal Wellfield EGS favorability and trust maps represent an integrated semi-quantitative summary of the results of this analysis, which was constrained by three parameters of interest for EGS (1) temperatures greater than 200–250 °C at depths of 1–5 km, (2) brittle rock capable of sustaining fractures at the depth of interest and (3) favorable stress regime at the depth of interest. The definition of these parameters for at any given site for EGS favorability can be achieved through

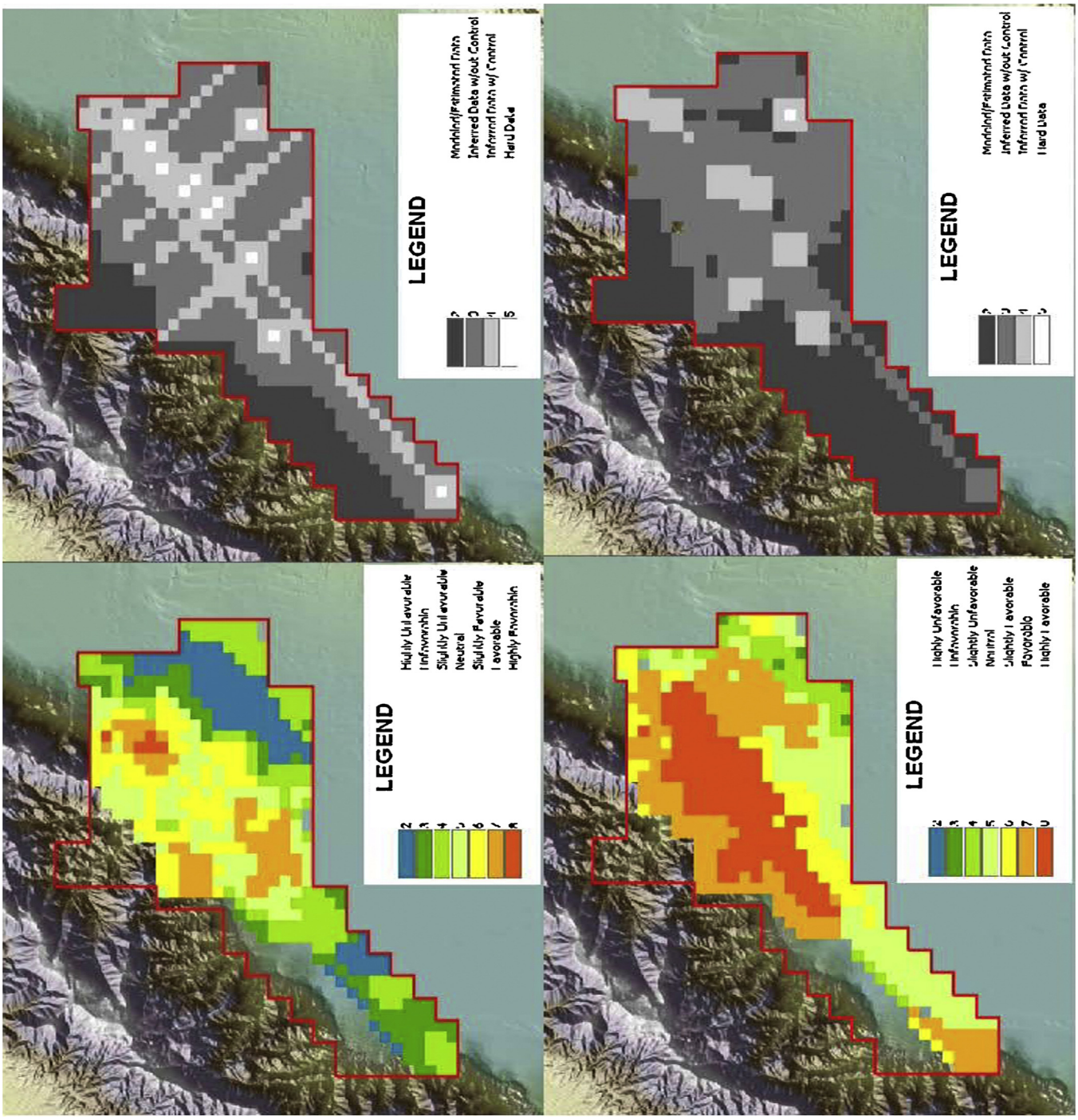

Fig. 9. EGS favorability maps (left) and associated trust maps (right); see text for an explanation. The upper figures are at −1 km above sea level or a depth of 2 km, while the lower figures are at −2.5 km above sea level, or a depth of 3.5 km. Trust values are presented in shades of black and white with the more reliable data cells in a lighter shade. The figure and caption are from Iovenitti et al. (2012) and AltaRock Energy Inc. (2014a). (For interpretation of the references to color in the text, the reader is referred to the web version of this article.)

the exploration techniques used and their integrated geoscientific analysis and synthesis to define a detailed conceptual model of the subsurface. The model provides the basis for a comprehensive delineation of the EGS favorability of a given site. Similarly, the trust maps reflect a semi-quantitative integrated confidence (i.e., trust) the geoscientist and/or the geoscientific team has in the data used to define each parameter of interest. This coupled approach provides an objective method to evaluate a geothermal site in a straightforward and well-documented manner. It should be noted that the methodology described for EGS can be readily adapted to hydrothermal systems by expanding the types of parameters considered in the analysis. For example, if a fractured hydrothermal system is being analyzed, permeability (i.e., permeability distribution) should be added to the parameters of interest.

During the preparation of this article, the question arose of whether EGS favorability could be predicted using the available baseline geoscience dataset without the benefit of the measured well temperature data. A CART sensitivity analysis was conducted

with and without the EV vertical stress, which was deemed by the project team (listed in Section 7) as a duplicative parameter since both temperature and vertical stress increase with depth in the DVGW. For the RVs of temperature, lithology, productive vs. non-productive hydrothermal cells and expected EGS favorable cells, r^2-values ranging from 0.611 to 0.841 were calculated considering all the EVs analyzed including vertical stress. Removing the EV vertical stress, the CART sensitivity analysis showed that r^2-values ranged from 0.615 to 0.769 using a variety of EVs for the same set of RVs. It is debatable whether dilatation should be used to predict EGS favorability since this study showed that structural dilatation zones are directly associated with the shallow thermal anomalies and the deep geothermal production and injection wells and as such is a predictor of the presence of a hydrothermal reservoir. In this study the project team (see Acknowledgements section) decided to also include dilatation in the prediction for a viable EGS area.

While this paper describes an EGS exploration assessment for the DVGW in the Basin and Range, the exploration techniques evaluated and the analysis conducted has widespread application for any type of EGS or hydrothermal setting because both the techniques and analyses conducted are fundamental in the evaluation of a geothermal system. Exploration techniques and analyses conducted for any given geothermal site, undoubtedly, may vary depending on the particulars of that site. However the general approach presented is applicable for any geothermal site.

Acknowledgements

The authors express their thanks to their colleagues on this project: Drs. Robert Karlin (gravity and magnetics task leader); Ileana Tibuleac (seismic task leader); David Blackwell (thermal task leader) and his post-doctoral researcher, Mahesh Thakur; Phil Wannamaker (MT task leader) and his post-doctoral researcher, Virginia Maris; Trenton Cladouhos (geology task leader); B. Mack Kennedy (geochemistry task leader); and Ed Isaaks (geostatistics task leader in the second part of this study) as well as Messrs. Al Waibel (geologic consultant) and Michael Swyer (GIS in later phases of the project). Matthew Clyne, Owen Callahan and Jon Sainsbury, co-authors on this paper were also the project GIS task leader for the phase of the project that is the subject of this paper. Owen Callahan assisted in generating GIS maps) and was also responsible for the 3D gridded model that was used in correlating the geology and geophysical model cross-sections. Jon Sainsbury, the project deputy, supported all aspects of the reported project results. The authors are also indebted Mr. Al Waibel for his review of this paper, Mr. Michael Swyer for details on CSC and Poly 3D and Drs. John Ziagos and Patrick Dobson. Comments by the latter were especially useful in expanding certain elements of this paper. Finally, the authors also express their appreciation for the co-funding provided for this study by the U.S. Department of Energy Geothermal Technologies Program and AltaRock Energy Inc., under the American Recovery and Reinvestment Act (ARRA) United States Department of Energy contract no. DE-EE000277.

References

Aimene, Y., Ouenes, A., 2015. Geomechanical modeling of hydraulic fractures interacting with natural fractures—validation with microseismic and tracer data from the Marcellus and Eagle Ford. Interpretation 3 (3), SU71–SU88, http://dx.doi.org/10.1190/INT-2014-0274.1.

AltaRock Energy Inc., 2014a. EGS Exploration Methodology Project using the Dixie Valley Geothermal System, Nevada as a calibration site part I—final scientific report baseline conceptual model, US Department of Energy DOE Award: DE-EE0002778, submitted to the National Geothermal Data Repository, 177pp.

AltaRock Energy Inc., 2014b. EGS Exploration Methodology Project using the Dixie Valley Geothermal System, Nevada as a calibration site part II—final scientific report baseline conceptual model, US Department of Energy DOE Award: DE-EE0002778, submitted to the National Geothermal Data Repository, 203pp.

Bell, J.W., Caskey, S.J., Ramelli, A.R., Guerrieri, L., 2004. Pattern and rates of faulting in the Central Nevada Seismic Belt, and paleoseismic evidence for prior beltlike behavior. Bull. Seismol. Soc. Am. 94 (August (4)), 1229–1254.

Benoit, D., 1999. Conceptual models of the Dixie Valley, Nevada Geothermal Field, Geothermal Resources Council (GRC) Transactions, vol. 23, pp. 505–511.

Biasi, G., Tibuleac, I., Preston, L., 2008. Regional resource area mapping in Nevada using the USArray Seismic Network, paper presented at the Geothermal Energy 2008 Conference and Expo, Reno, NV, October 5–8.

Blackwell, D.D., Bergman, S., Goff, F., Kennedy, B.M., McKenna, J.R., Richards, M.C., Smith, R.P., Waibel, A.F., Wannamaker, P., 2005. Description, synthesis, and interpretation of the thermal regime, geology, geochemistry and geophysics of the Dixie Valley, Nevada Geothermal System. In: Blackwell, D.D., Smith, R.P. (Eds.), unpublished DRAFT DOE Technical Report, 195pp.

Blackwell, D.D., Leidig, M., Smith, R.P., 2002. Regional geophysics of the Dixie Valley Area: xxample of a large Basin and Range geothermal resource, Geothermal Resources Council Transactions, vol. 26, pp. 519–522.

Blackwell, D.D., Smith, R.P., Richards, M.C., 2007. Exploration and development at Dixie Valley, Nevada, summary of DOE studies. In: 32nd Workshop on Geothermal Reservoir Engineering Stanford University, Stanford, California, January 22–24.

Blackwell, D.D., Wisian, K.W., Benoit, D., Gollan, B., 1999. Structure of the Dixie Valley Geothermal System, a typical Basin and Range geothermal system, from thermal and gravity data, Geothermal Resources Council Transactions, vol. 23, 7pp.

Caskey, S.J., Wesnousky, S.G., Zhang, P., Slemmons, D.B., 1954. Surface faulting of the Fairview Peak (Ms 7.2) and Dixie Valley (Ms 6.8) earthquakes, Central Nevada. Bull. Seismol. Soc. Am. 86 (3), 761–787.

Caskey, S.J., Wesnousky, S.G., 2000. Active faulting and stress redistributions in the Dixie Valley, Beowawe, and Bradys geothermal fields: implications for geothermal exploration in the Basin and Range. In: Proceedings 25th Workshop on Geothermal Reservoir Engineering Stanford University, California, January 24–26, 16pp.

Hickman, S., Zoback, M., Benoit, R., 1998. Tectonic controls on reservoir permeability in the Dixie Valley, Nevada Geothermal Field. In: Proceedings 23rd Workshop on Geothermal Reservoir Engineering Stanford University, California, January 26–28, 8pp.

Hickman, S.H., Zoback, M.D., Barton, C.A., Benoit, R., Svitek, J., Summers, R., 2000. Stress and permeability heterogeneity within the Dixie Valley Geothermal Reservoir: recent results from well 82-5. In: Proceedings 25th Workshop on Geothermal Reservoir Engineering Stanford University, Stanford, California, January 24–26, 10pp.

Iovenitti, J.L., Blackwell, D.D., Sainsbury, J.S., Tibuleac, I.M., Waibel, A.F., Cladouhos, T.T., Karlin, R., Kennedy, B.M., Isaaks, E., Wannamaker P.E., Clyne, M.T., Callahan, O.C., 2011. EGS Exploration Methodology Development using the Dixie Valley Geothermal District as a calibration site, a progress report, GRC Transactions, vol. 35, pp. 389–395.

Iovenitti, J., Blackwell, D., Sainsbury, J., Tibuleac, I., Waibel, A., Cladouhos, T., Karlin, R., Isaaks, E., Clyne, M., Ibser, F.H., Callahan, O., Kennedy, B.M., Wannamaker, P., 2012. Towards developing a calibrated EGS Exploration Methodology using the Dixie Valley Geothermal System, Nevada. In: Proceedings 37th Eighth Workshop on Geothermal Reservoir Engineering Stanford University, Stanford, California, January 30–February 1, SGP-TR-194, 15pp.

Iovenitti, J., Sainsbury, J., Tibuleac, I., Karlin, R., Wannamaker, P., Maris, V., Blackwell, D., Thakur, M., Ibser, F.M., Lewicki, J., Kennedy, B.M., Swyer, M., 2013. EGS Exploration Methodology Project using the Dixie Valley Geothermal System, Nevada, status update. In: Proceedings 38th Workshop on Geothermal Reservoir Engineering Stanford University, Stanford, California, February 11–13, SGP-TR-198, 10pp.

Iovenitti, J., Tibuleac, I., Wannamaker, P., Karlin, R., Ibser, F.H., Blackwell, D., Sainsbury, J., 2015. Development of an Engineered Geothermal System Exploration Methodology using the Dixie Valley Geothermal Area, Nevada USA, as a laboratory calibration site system, invited paper to Proceedings World Geothermal Congress, Melbourne, Australia, 19–25 April, 15pp.

Kennedy, B.M., van Soest, M.C., 2006. A helium isotope perspective on the Dixie Valley, Nevada, hydrothermal system. Geothermics 35, 26–43.

Lawrence, R.L., Wright, A., 2001. Rule-based classification systems using Classification and Regression (CART) analysis. Photogramm. Eng. Remote Sens. 67 (10), 1137–1142.

Lutz, S.J., Moore, J.N., Benoit, D., 1997. Geologic framework of Jurassic Reservoir Rocks in the Dixie Valley Geothermal Field, Nevada: implications from hydrothermal alteration and stratigraphy. In: Proceedings 22nd Workshop on Geothermal Reservoir Engineering Stanford University, California, January 27–29, 9pp.

Mase, C.W., Sass, J.H., 1980. Heat flow from the western arm of the Black Rock Desert, Nevada, US Geological Survey, Open-File Report 80-1238.

MIT, 2006. The future of Geothermal Energy. Impact of Enhanced Geothermal Systems (EGS) on the United States in the 21st Century, Assessment by a Massachusetts Institute of Technology-led interdisciplinary panel (J.F. Tester, Chairman), 372pp, http://geothermal.inel.gov/publications/future_of_geothermal_energy.pdf.

Page, B.M., 1965. Preliminary geologic map of a part of the Stillwater Range, Churchill County, Nevada, Nevada Bureau of Mines, Map 28.

Reed, M.J., 2007. An investigation of the Dixie Valley Geothermal Field, Nevada, using temporal moment analysis of tracer tests. In: Proceedings 32nd Workshop on Geothermal Reservoir Engineering Stanford University, Stanford, California, January 22–24, 8pp.

Smith, R.P., Grauch, V.J.S., Blackwell, D.D., 2002. Preliminary results of a high-resolution aeromagnetic survey to identify buried faults at Dixie Valley, Nevada, GRC Transactions, vol. 26, pp. 543-546.
Smith, R.P., Wisian, K.W., Blackwell, D.D., 2001. Geologic and geophysical evidence for intra-basin and footwall faulting at Dixie Valley, Nevada, GRC Transactions, vol. 25, pp. 323-326.
Speed, R.C., 1976. Geologic map of the Humboldt Lopolith and surrounding terrane, The Geologic Society of America, Inc., Map and Chart Series MC-14, 4pp.
Stewart, J.H., Carlson, J.E., 1978. Geologic map of Nevada, U.S. Geological Survey, 1:500,000 scale.
Swyer, M.W., Davatzes, N.C., 2013. Evaluating the role of the Rhyolite Ridge Fault System in the Desert Peak Geothermal Field with robust sensitivity testing through boundary element modeling and likelihood analysis. In: Proceedings 38th Workshop on Geothermal Reservoir Engineering Stanford University, Stanford, California, February 11–13.
USGS, 2008, Assessment of Moderate- and High-Temperature Geothermal Resources of the United States, U.S. Department of the Interior, United States Geological Survey, Fact Sheet 2008–3082, 4pp.
Waibel, A.F., 1987. An overview of the geology and secondary mineralogy of the high temperature geothermal systems in Dixie Valley, Nevada. GRC Transactions 11, 479–486.
Waibel, A.F., 2011. Structural controls on the location of geothermal cells in and adjacent to Dixie Valley, Nevada, GRC Transactions, vol. 35, pp. 1045-1052.
Wannamaker, P.E., Doerner, W.M., Hasterok, D.P., 2007. Integrated dense array and transect MT surveying at Dixie Valley Geothermal Area, Nevada; structural controls, hydrothermal alteration and deep fluid sources. In: Proceedings 32nd Workshop on Geothermal Reservoir Engineering Stanford University, California, January 22–24, 6pp.
Wannamaker, P.E., Doerner, W.M., Hasterok, D.P., 2006. Cryptic faulting and multi-scale geothermal fluid connections in the Dixie Valley-Central Nevada Seismic Belt Area: implications from MT resistivity surveying. In: Proceedings 31st Workshop on Geothermal Reservoir Engineering Stanford University, California, January 30–February 1, 8pp.
Wallace, R.E., Whitney, R.A., 1984. Late Quaternary history of the Stillwater seismic gap, Nevada. Bull. Seismol. Soc. Am. 74 (1), 301–314.
Wooden, J.L., Kistler, R.W., Tosdal, R.M., 1999. Strontium, lead, and oxygen isotopic data for granitoid and volcanic rocks from the Northern Great Basin and Sierra Nevada, California, Nevada and Utah, USGS Open-file Report, 99-569, 15pp.